Geophysical Journal International

Geophys. J. Int. (2015) **203,** 366–372
GJI Seismology

doi: 10.1093/gji/ggv319

A hypocentral version of the space–time ETAS model

Yicun Guo,[1] Jiancang Zhuang[2] and Shiyong Zhou[1]

[1]*Department of Geophysics, School of Earth and Space Science, Peking University, Beijing* 100871, *China. E-mail: guoyicun@pku.edu.cn*
[2]*Institute of Statistical Mathematics,* 10-3 *Midori-cho, Tachikawa, Tokyo* 190-8562, *Japan*

Accepted 2015 July 27. Received 2015 July 25; in original form 2015 May 7

SUMMARY

The space–time Epidemic-Type Aftershock Sequence (ETAS) model is extended by incorporating the depth component of earthquake hypocentres. The depths of the direct offspring produced by an earthquake are assumed to be independent of the epicentre locations and to follow a beta distribution, whose shape parameter is determined by the depth of the parent event. This new model is verified by applying it to the Southern California earthquake catalogue. The results show that the new model fits data better than the original epicentre ETAS model and that it provides the potential for modelling and forecasting seismicity with higher resolutions.

Key words: Probabilistic forecasting; Probability distributions; Earthquake interaction, forecasting and prediction; Seismicity and tectonics; Statistical seismology.

1 INTRODUCTION

Clustering is one of the most important characteristics of seismicity. Seismicity is generally divided into two parts: a background part and a cluster part; the former is useful in long-term earthquake forecasts whereas the latter is useful for short-term earthquake forecasts. Early studies of temporal clustering of earthquakes date back to 1894, when the famous Omori law was proposed for the first time by Omori (1895). Based on this formula and other empirical laws, Ogata (1988) developed the Epidemic-Type Aftershock Sequence (ETAS) model and then generalized it to space–time (Ogata 1998). This model describes the features of earthquake clustering of foreshocks, main shocks and aftershocks.

In the past decade or so, this model has been greatly developed (see Console & Murru 2001; Console *et al.* 2003; Zhuang *et al.* 2002, 2004, 2008; Ogata 2004; Zhuang *et al.* 2005; Console *et al.* 2006; Marzocchi & Lombardi 2009; Helmstetter *et al.* 2006; Werner *et al.* 2011; Zhuang 2011). Among these works, Zhuang *et al.* (2002) introduced a stochastic declustering algorithm to objectively extract background seismicity from an earthquake catalogue. This algorithm provides us with the probability description of any two earthquakes in a catalogue; based on this probability we can quantify the triggering effect of a foreshock to its main shock, or of a main shock to any aftershock.

The time-varying seismicity rate function in the ETAS model is written as

$$\lambda(t,x,y|\mathcal{H}_t) = \frac{\Pr\{N(\mathrm{d}t\times\mathrm{d}x\times\mathrm{d}y)\geq 1\mid \mathcal{H}_t\}}{\mathrm{d}t\times\mathrm{d}x\times\mathrm{d}y} = \nu\mu(x,y)+\sum_{i:t_i<t}\xi(t-t_i,x-x_i,y-y_i;M_i), \quad (1)$$

where $\mu(x, y)$ is the background seismicity rate, ν is a relaxation parameter to speed the convergence in the maximum likelihood estimation procedure, $\mathcal{H}_t$ includes information of the events that occur before time t (Zhuang *et al.* 2002, 2004, 2005, 2008; Zhuang & Ogata 2006), and i runs over all the events in the observation history $\mathcal{H}_t$. The cluster seismicity rate of an earthquake with magnitude M, $\xi(t, x, y; M)$, has the formulation

$$\xi(t,x,y;M) = \kappa(M)g(t)f(x,y;M), \quad (2)$$

where $\kappa(M) = Ae^{\alpha(M-M_C)}$ is the expected number of events triggered by an event of magnitude M, with M_C being the magnitude threshold, and the functions $g(t) = \frac{p-1}{c}(1+\frac{t}{c})^{-p}$ and $f(x,y;M) = \frac{q-1}{\pi D^2 e^{\gamma(M-M_C)}}(1+\frac{x^2+y^2}{D^2e^{\gamma(M-M_C)}})^{-q}$ are normalized time and space probability density functions (pdfs), respectively.

Although the 2-D epicentre ETAS model is widely used in many applications, a 3-D model incorporating earthquake hypocentres has been required but has not yet been developed. A direct way of including the focal depths in a 3-D model is to add the depth dimension in the space pdf in f. However, this makes the normalization of the space pdf very difficult to treat because the integration of $f(x, y, z)$ is limited in the seismogenic layer and the normalizing factor of the generalized space pdf depends on the depth of the parent. Thus it is necessary to treat the focal depth separately from the longitude and the latitude. Kagan (2007) generalized the epicentre χ distribution into a hypocentre density $\phi(r|p) = \frac{r}{p\sqrt{2\pi}}\{\exp[-\frac{(r-p)^2}{2}] - \exp[-\frac{(r+p)^2}{2}]\}$ for analysing earthquake location errors, and the number of events is the integral value in a sphere of radius R, centred on the hypocentre of the parent. Mai *et al.* (2005) used a gamma distribution in modelling hypocentres, with the integral domain of the spatial pdf ranging from 0 to $+\infty$. Both Kagan (2007) and Mai *et al.* (2005) regarded the hypocentre location as ranging to ∞ in their pdfs. Since earthquakes usually occur in the seismogenic layer, from surface to a specific depth depending on the local tectonic background, such treatments may not be ideal in describing earthquake hypocentres.

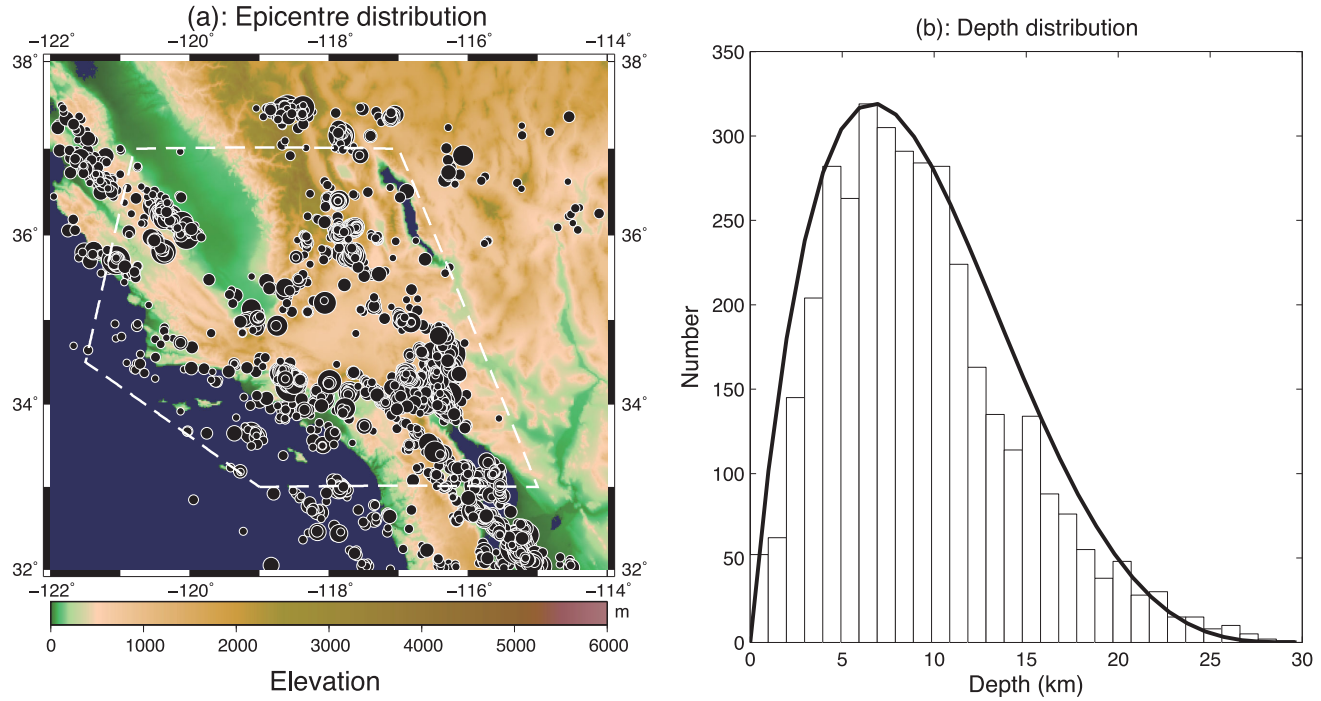

Figure 1. (a) Epicentre distribution of earthquakes above magnitude 3.5 from Southern California. The white-dashed polygon represents the region for model fitting; its vertices are (−119.0, 33.0), (−115.0, 33.0), (−117.0, 37.0), (−120.8, 37.0) and (−121.5, 34.5). The total number of earthquakes is 3678, and 2002 of these are located within the white polygon. (b) Histogram of earthquake depths. The solid line denotes the shape of the beta distribution $B(2.0, 4.5)$, corresponding to eq. (5) with $\eta = 2.5$, $z' = 12$ km.

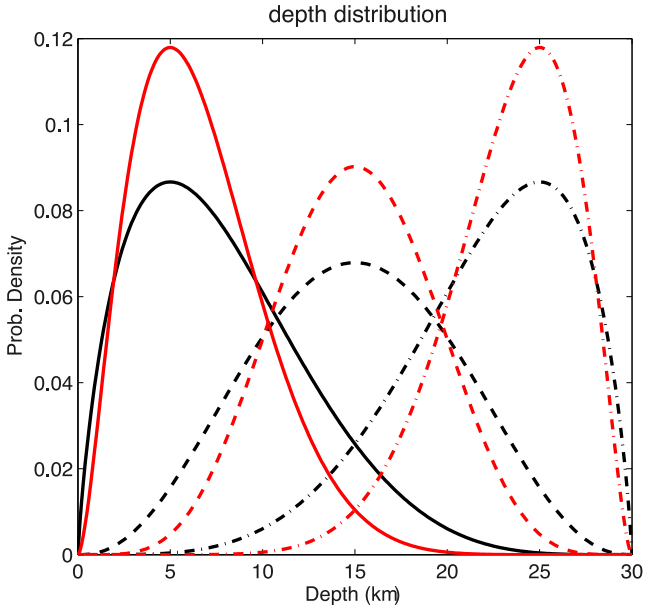

Figure 2. Examples of the distributions in eq. (5). The black and red lines represent $\eta = 5$ and $\eta = 10$ in eq. (5), respectively. The solid, dashed, and dot-dashed lines are depths of the main shocks at 5, 15, and 25, respectively.

Before proposing a proper density function, we inspected the characteristics of the focal depth distribution in the catalogue. Fig. 1(a) gives the locations of M3.5+ earthquakes in the Southern California Earthquake Data Center (SCEDC) catalogue; details of this catalogue are given in Section 3. From Fig. 1(b), we can see that earthquakes usually occur in the crust layer and most of their hypocentres are located at depth less than tens of kilometres. For the sake of simplicity, we exclude those earthquakes with deeper hypocentres than the thickness of the seismogenic layer, H, in our analyses. In the 3-D ETAS model, the depth pdf should have the following characteristics: (a) The seismicity beyond a depth of 0 km and H km is zero; (b) the nearer two earthquake hypocentres are, the higher is the probability of the latter event triggered by the previous one; (c) the integration of the depth pdf from 0 to H should be 1; that is, the triggering abilities of main shocks are limited in the seismogenic layer. In the following, we use the beta distribution, which satisfies the above prerequisites, as the depth distribution in the formulation of a hypocentral ETAS model, and we validate this treatment through stochastic reconstruction.

2 THE 3-D ETAS MODEL

In our 3-D ETAS model, the time-varying seismicity rate function is written as

$$\lambda(t, x, y, z|\mathcal{H}_t) = \mu(x, y, z) + \sum_{i:t_i<t} \xi(t - t_i, x - x_i, y - y_i, z - z_i; M_i, z_i), \quad (3)$$

where z_i is the focal depth of a parent event. The second part, that is, the cluster seismicity in eq. (3), is

$$\xi(t, x, y, z; M, z') = \kappa(M)g(t)f(x, y; M)h(z, z'), \quad (4)$$

where κ, g and f are the same as in eq. (2), and the focal depths obey a beta distribution:

$$h(z; z') = \frac{\left(\frac{z}{Z}\right)^{\eta\frac{z'}{Z}}\left(1 - \frac{z}{Z}\right)^{\eta\left(1-\frac{z'}{Z}\right)}}{Z\,B\left(\eta\frac{z'}{Z} + 1, \eta\left(1 - \frac{z'}{Z}\right) + 1\right)}, \quad (5)$$

with z/Z denoting the focal depths normalized by the thickness of seimogenic layer Z, z' being the depth of the main shock, and $B(p, q)$ being the beta function

$$B(p,q) = \int_0^1 t^{p-1}(1-t)^{q-1}\mathrm{d}t. \tag{6}$$

We neglect events beyond the seismogenic layer Z, since deep earthquakes in the subducting zone have a different clustering feature than that of the ETAS model. The parameter η controls how the triggered events concentrate at the depth of the parent event: a big η means a high concentration and $\eta = 0$ means a uniform distribution (Fig. 2).

We use the maximum likelihood procedure to estimate the parameters in the 3-D ETAS model. The log-likelihood function (*cf.* Daley & Vere-Jones 2003, chap. 7) is

$$\log L(\boldsymbol{\theta}) = \sum_{j:(t_j,x_j,y_j,z_j)\in S\times[T_1,T_2]\times Z} \log\lambda(t_j, x_j, y_j, z_j|\mathcal{H}_{t_j}) - \iiint_S \int_0^Z \int_{T_1}^{T_2} \lambda(t, x, y, z|\mathcal{H}_t)\mathrm{d}t\,\mathrm{d}z\,\mathrm{d}x\,\mathrm{d}y, \tag{7}$$

where $\theta = (\nu, A, \alpha, c, p, D, q, \gamma, \eta)$ are the model parameters, and j runs over all events in the study region S, the depth range Z, and the time period $[T_1, T_2]$. Note that the time–space range for j can be smaller than that for i in eq. (3) for the large events beyond but near the study area. Since the background is also unknown, an iterative algorithm (Zhuang *et al.* 2002) is used to estimate the background rate and the model parameters simultaneously.

3 DATA SELECTION AND ANALYSES

We used the earthquake catalogue from Southern California (SC), during the period from 1981 January 1 to 2011 June 30, in the range of 114°–122°E, 32°–38°N. We selected the earthquakes above a magnitude threshold of 3.5 after considering the incompleteness of aftershocks immediately after the large main shocks. The region for estimation is the polygon shown in Fig. 1(a). Since most of earthquakes in SC are shallow events, the depth of the seismogenic layer is taken as 30 km here; i.e. those events deeper than 30 km are neglected in our analyses. Fig. 1(b) shows the depth distribution of all the events in the catalogue. Most of earthquakes occur in the upper crust layer (shallower than 15 km), with only a very tiny portion of all earthquakes at depths ≥30 km.

4 RESULTS

4.1 Data fittings

Table 1 shows the results from fitting the 2-D and 3-D ETAS models to the data. However, these two models cannot be compared directly through their likelihoods since the observation data set for the 2-D model is $\{(t_i, x_i, y_i, m_i)\}$ and that for the 3-D model is $\{(t_i, x_i, y_i, z_i, m_i)\}$. Kagan (1991) used a histogram of the depth distribution of hypocentres in a likelihood analysis of earthquake catalogues; here we follow the same technique used to modify the likelihood of the 2-D model. We incorporated the depth information in the 2-D likelihood to contrast ETAS models with two null hypotheses: (a) earthquakes are distributed uniformly in depth; (b) earthquakes are distributed empirically just the same as the observational history. For the latter case, we used the histogram of depths of all events in the catalogue to estimate the depth distribution: $h'(z) = \frac{n}{N\Delta z}$, where n is the number of events in the depth range $(z, z + \Delta z)$. Note that case (b) degenerates to case (a) when Δz takes the thickness of the whole seismogenic layer Z. Based on the above idea, we corrected the likelihood of the 2-D ETAS model by using the following two equations:

$$\log L_u = \log L_{2D} - N\log Z, \tag{8}$$

$$\log L_e = \log L_{2D} + \sum_{i=1}^{N_{\Delta z}} n_i \log\frac{n_i}{N\Delta z}; \tag{9}$$

that is, $\log L_u$ and $\log L_e$ are the log-likelihood function values when the uniform and empirical depth distributions are attached to the 2-D ETAS models, respectively, but independent of other components. In eqs (8) and (9), $N_{\Delta z} = Z/\Delta z$ is the total number of discrete depths, n_i is the number of events located in $[z_i, z_i + \Delta z]$, $\log L_{2D}$ is the likelihood for the 2-D ETAS model, N is the number of earthquakes in the target area, and Z denotes the maximum depth that we used in the model. By using eqs (8) and (9), we obtained log-likelihood values of −4761.4 for the 2-D model with a uniform depth distribution and −3454.3 for the 2-D model with an empirical depth distribution, both of which are much smaller than the likelihood value of −2904.6 for the 3-D ETAS model.

Except for the log-likelihood values, the common parameters of the 2-D and 3-D models are slightly different. Such differences can be interpreted in the following way: The total seismicity is the summation of background and cluster parts; a change in the latter part affects the former part, which in turn affects the parameters of the cluster part in spite of the fact that we treated the depth pdf separately in the cluster seismicity. Especially, an α value that is smaller in the 3-D ETAS model than in the 2-D ETAS model shows that the triggering ability of larger earthquakes of the 3-D model is less than that of the 2-D model. This is because, when we add the depth dimension in the 3-D model, events far away from the hypocentres of large earthquakes are more likely to be treated as being triggered by small earthquakes whose hypocentres are closer.

4.2 Validation through stochastic reconstruction

We used stochastic reconstruction to verify our new model. The stochastic reconstruction method (Zhuang *et al.* 2004) helps us visualize the data fitting. The depth density $h(z; z')$ can be reconstructed for a given z' by using the following equation:

$$\hat{h}(z;z') = \frac{\sum_{ij}\rho_{ij} I(|z_j - z_i| \in [z - \frac{\Delta z}{2}, z + \frac{\Delta z}{2}]) I(z_i \in [z' - \frac{\Delta z'}{2}, z' + \frac{\Delta z'}{2}])}{\Delta z \sum_{ij}\rho_{ij} I(z_i \in [z' - \frac{\Delta z'}{2}, z' + \frac{\Delta z'}{2}])}. \tag{10}$$

Table 1. Results of data fittings from the 2-D and 3-D ETAS models.

Model	A	c	α	p	D^2	q	γ	η	$\log L$	$\log L_u/\log L_e$
2dETAS	0.302	0.013	1.40	1.16	0.88×10^{-5}	1.58	1.62	–	+2047.8	−4761.4/−3454.3
3dETAS	0.364	0.013	1.18	1.17	0.10×10^{-4}	1.50	1.45	31.7	−2904.6	–

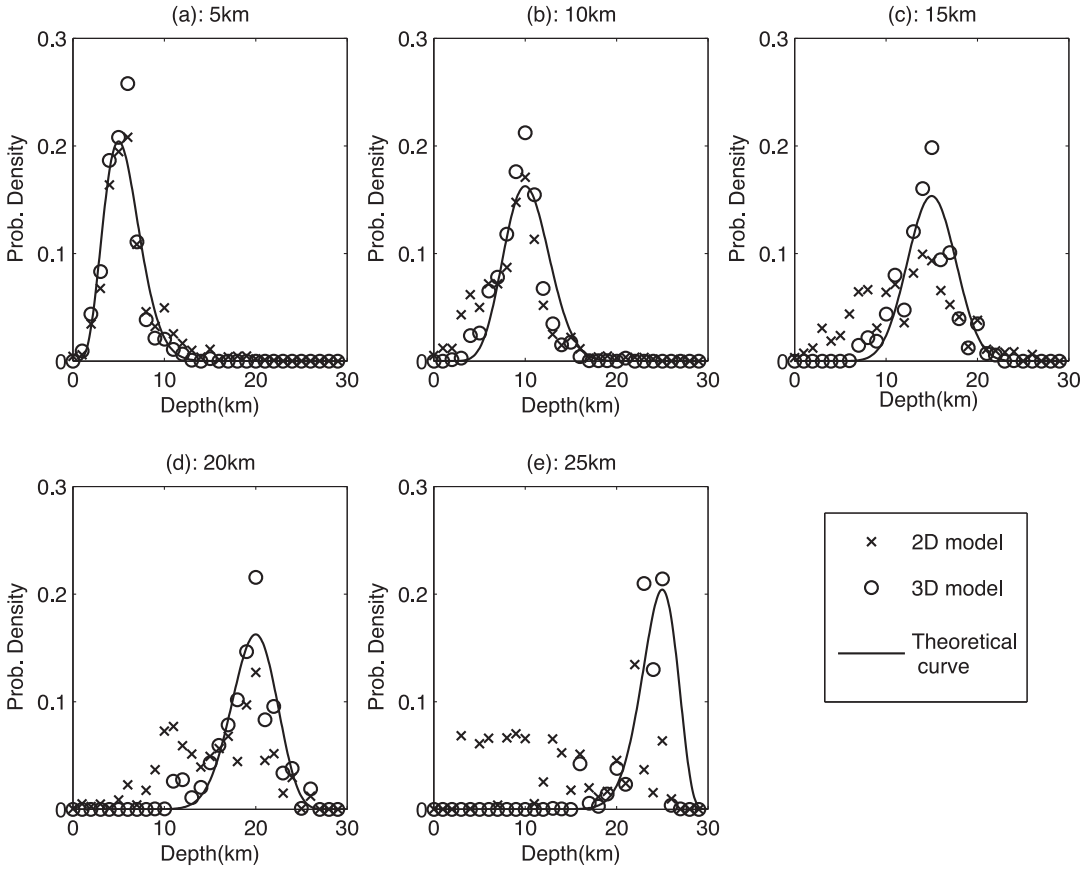

Figure 3. Reconstructed relationship between aftershock frequencies versus depths. Five depths of main shocks are selected to show the results here. Solid lines denote the theoretical curves of $h(z)$.

In Fig. 3, we show the reconstructed aftershock distribution at five depths of z'. In the 5- and 10-km cases, we can see that although we do not incorporate focal depths in the 2-D model, the reconstruction results are almost the same as those from the 3-D model. For the deeper 20- and 25-km depths, results from the 2-D and 3-D models are less consistent because only a few events occur at these depths. Because the 2-D ETAS model does not incorporate focal depths, it is not surprising that the reconstructed points for 15-, 20- and 25-km parent-shock depths tend to be distributed uniformly in Fig. 3. However, at 5- and 10-km depths, the reconstructed depth density functions have distributions very similar to those from the 3-D ETAS model. This occurs because, although we do not take focal depths into consideration in the 2-D ETAS model, two events of greatly differing depth are also likely to have epicentres that are far from each other, and vice versa, since the epicentres are the projections of hypocentres on the Earth's surface. In other words, the agreement of the 2-D results with the 3-D theoretical curves indicates that the beta distribution is quite appropriate for describing triggering effects of earthquakes in the depth dimension.

4.3 Reconstruction of magnitude, time, and epicentre distributions

Schoenberg (2015) pointed out that modification of the spatial term of the ETAS model in Ogata (1998) can result in substantial changes to the parameters of temporal and magnitude terms, since the total seismicity rate function λ is not separable in x and y. Similarly in our 3-D-hypocentre ETAS model, although we only modify the 2-D-epicentre ETAS model by multiplying a depth distribution in the clustering seismicity, it is not surprising that all the parameters in Table 1 change more or less because λ is not multiplicative in depth dimension z. Thus any changes of parameter values resulting from the depth dimension that we add could also affect distributions of other dimensions. Stochastic reconstruction helps us understand to what extent the triggering ability, time and epicentre pdfs of the 3-D ETAS model differ from those of the 2-D ETAS model. All of these distributions can be reconstructed by using the following equations from Zhuang *et al.* (2004):

$$\hat{\kappa}(M) = \frac{\sum_i \sum_j \rho_{ij} I(M_i \in [M - \Delta M/2, M + \Delta M/2])}{\sum_i I(M_i \in [M - \Delta M/2, M + \Delta M/2])}, \tag{11}$$

$$\hat{g}(t) = \frac{\sum_{i,j} \rho_{ij} I(t_j - t_i \in [t - \Delta t/2, t + \Delta t/2])}{\Delta t \sum_{i,j} \rho_{ij}}, \tag{12}$$

$$\hat{f}_R(r) = \frac{\sum_{i,j} \rho_{ij} I(r_{ij} \in [r - \Delta r/2, r + \Delta r/2])}{\Delta r \sum_{i,j} \rho_{ij}}, \tag{13}$$

where ρ_{ij} is the probability of event j triggered by previous event i, I is the index function taking 1 if the statement is true and r_{ij} is the standardized distance defined by

$$r_{ij} = \sqrt{\frac{(x_j - x_i)^2 + (y_j - y_i)^2}{D^2 e^{\gamma(M_i - M_C)}}}. \tag{14}$$

Figs 4(a)–(c) show the reconstructed results from the 2-D and 3-D ETAS models.

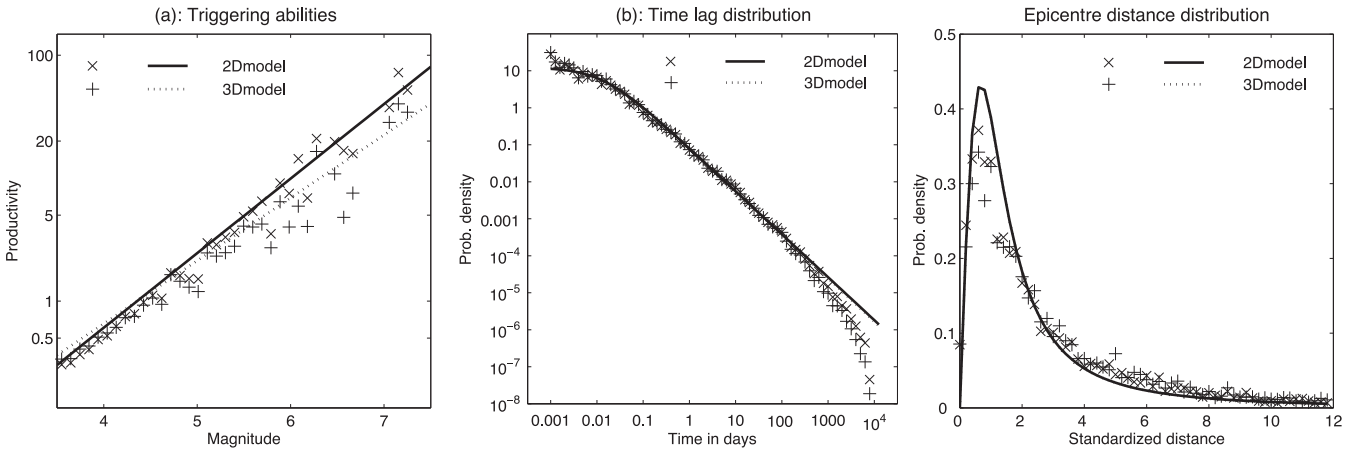

Figure 4. Reconstruction results of (a) the triggering abilities, (b) the time lag distribution, and (c) the epicentre distribution. Theoretical curves of $\kappa(M)$ time and space pdfs are plotted by solid and dashed lines for the 2-D and 3-D models, respectively.

(1) In Fig. 4(a), the exponential law fits $\kappa(M)$ well in the 2-D model, and the fitting becomes worse in the 3-D model, especially in the large-magnitude interval. Note that the reconstructed curves tend to be lower than the theoretical ones for both models. By comparing the theoretical curves of the 3-D and 2-D models, we note that the triggering abilities of large events are lower whereas those of small events are higher in the 3-D case. This is because, for large main shocks, an overall η value has limits in triggering aftershocks in the whole seismogenic layer. More importantly, since earthquake depth has the biggest uncertainty in the hypocentral coordinates, we have to ensure that the number of events is large enough to get stable results from the 3-D model. Meanwhile, the influence of depth uncertainty can also be reflected in the results, and it becomes more significant in case of catalogues compiled from a sparser seismological network.

(2) Fig. 4(b) shows the time lag distributions of the two models. Their results are almost the same and fit the theoretical curves very well. The main discrepancy is at the ends of the curves, where the time difference is >1000 days. The decrease at the tail is due to the absence of events beyond the observation period. The consistency at short time lags (0.01 day) indicates that the completeness of the catalogue above magnitude 3.5 is quite good. On the whole, the agreement between theoretical curves and reconstructed points from 0.01 to 1000 days shows a good fit to the Omori–Utsu law.

(3) From Fig. 4(c), we can see that the theoretical curve of the 3-D model completely overlaps with the 2-D curve, so the difference of reconstructed points of the two models can be neglected.

In summary, by reconstruction, we can see that the 3-D ETAS model preserves the time and epicentre distributions of the 2-D ETAS model very well, and bigger change occurs in the triggering ability function, as also indicated in the maximum likelihood estimates of parameters.

4.4 Background seismicity estimation

Background seismicity is an important parameter obtained from statistical models because it is related to the tectonic loading rate. In our ETAS model, it is assumed to be constant in time and to vary in space. As mentioned in Section 2, we can estimate the background seismicity in the 2-D ETAS model through the algorithm introduced by Zhuang *et al.* (2002). The total seismicity rate is estimated by the variable kernel estimation method as follows:

$$\hat{m}_1(x, y) = \frac{1}{T} \sum_{j=1}^{N} k_{d_j}(x - x_j, y - y_j), \tag{15}$$

where $\hat{m}_1(x, y)$ is the total spatial intensity function (first-order moment density) and d_j represents the bandwidth of event j in the Gaussian kernel function $k_{d_j}(x - x_j, y - y_j)$ given by

$$k_{d_j}(x, y) = \frac{1}{2\pi d_j} \exp\left\{-\frac{x^2 + y^2}{2d_j^2}\right\}. \tag{16}$$

Then the background seismicity rate can be calculated by using

$$\hat{\mu}(x, y) = \frac{1}{T} \sum_{j=1}^{N} \phi_j k_{d_j}(x - x_j, y - y_j), \tag{17}$$

where ϕ_j is the probability of event j being a background event from the stochastic decluster algorithm (Zhuang *et al.* 2002). For the 3-D ETAS model, the corresponding total seismicity rate at a specific depth is written as

$$\hat{m}_1'(x, y, z) = \frac{1}{T} \sum_{j=1}^{N} k_{d_j}(x - x_j, y - y_j) \times \frac{\left(\frac{z}{Z}\right)^{d_z \frac{z_j}{Z}} \left(1 - \frac{z}{Z}\right)^{d_z\left(1 - \frac{z_j}{Z}\right)}}{B\left(d_z \frac{z_j}{Z} + 1, d_z\left(1 - \frac{z_j}{Z}\right) + 1\right)}, \tag{18}$$

where d_z is the fixed bandwidth in the depth dimension. The background seismicity rate can be calculated in a similar way as the 2-D case by multiplying the background probabilities of events obtained from declustering in the 3-D model.

Fig. 5 shows background seismicity rates estimated from 2-D and 3-D ETAS models. The 2-D result can be taken as the integration of 3-D results from Z to the Earth's surface. The seismicity rates at specific depths provide us with more earthquake hazard information in the depth dimension. From the results of the Southern California catalogue, we can see that most earthquakes occur in the upper layer of the crust and that the most active seismicity occurs at a depth of ∼10 km.

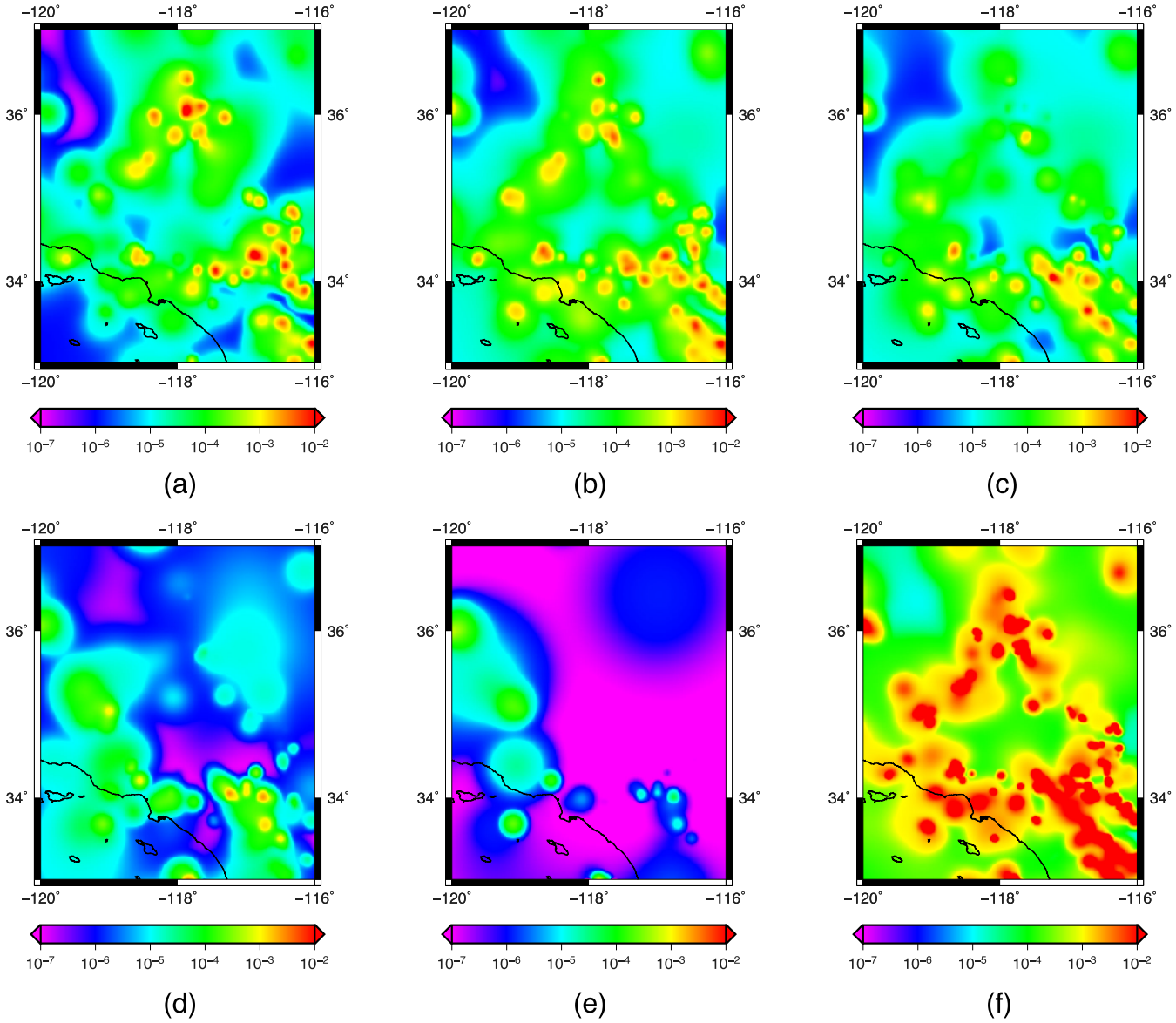

Figure 5. Background seismicity rate estimated from 3-D and 2-D ETAS models. (a), (b), (c), (d), and (e) are from the 3-D model with depths of 5, 10, 15, 20 and 25 km, respectively. (f) is from the 2-D model. The background seismicity values are in events day^{-1} deg^{-2}, and contours are plotted on a logarithmic scale.

5 CONCLUSIONS

We extended the 2-D-epicentre ETAS model to a 3-D-hypocentre ETAS model to analyse earthquake hypocentres by introducing a beta distribution for modelling the earthquake depth. The 3-D model provides the potential for forecasting seismicity with high resolution. The stochastic reconstruction results from the SCEDC catalogue indicate that the 3-D model performs better in data fittings than the 2-D model. Whether this beta distribution of depth pdf is appropriate for other regions, for instance, the more complicated JMA catalogue, should be verified in future studies. The reconstructed results of the 3-D ETAS model in Fig. 3 have a fixed triggering band (∼10 km) in the depth pdf. This band may not be big enough for large earthquakes since their aftershocks may extend to the whole seismogenic layer. Further research taking into account the scaling of earthquake magnitudes in depth triggering should be made. One possible way to solve this problem is to apply finite sources instead of point sources for large earthquakes, as implemented by Guo *et al.* (2015) for the 2-D ETAS model. The utility of the 3-D ETAS model is limited because reliable and complete hypocentre catalogues are currently not available all over the world; in fact, the Southern California catalogue is perhaps the best. Therefore, obtaining robust results from the 3-D model will require a local dense seismological network to locate earthquake hypocentres.

ACKNOWLEDGEMENTS

The data used in the present study are available from the Southern California Earthquake Data Center (http://service.scedc.caltech.edu/ftp/catalogs/SCEC_DC/). This research was supported in part by JSPS Grants-in-Aid C25300052, A26240004 and B26280006; NSFC Grant 41274052. The authors would like to thank Prof Yosihiko Ogata from ISM and Prof Naoshi Hirata and

Dr Hiroshi Tsuruoka from ERI, Univerisity of Tokyo, for helpful discussions. We would also like to thank the two reviewers, Yan Y. Kagan and Rodolfo Console, for their encouragement and constructive comments.

REFERENCES

Console, R. & Murru, M., 2001. A simple and testable model for earthquake clustering, *J. geophys. Res.,* **106**(B5), 8699–8711.

Console, R., Murru, M. & Lombardi, A.M., 2003. Refining earthquake clustering models, *J. geophys. Res.,* **108**(B10), 2468, doi:10.1029/2002JB002130.

Console, R., Rhoades, D.A., Murru, M., Evison, F.F., Papadimitriou, E.E. & Karakostas, V., 2006. Comparative performance of time-invariant, long-range and short-range forecasting models on the earthquake catalogue of Greece, *J. geophys. Res.,* **111**(B09), 304, doi:10.1029/2005JB0044113.

Daley, D.D. & Vere-Jones, D., 2003. *An Introduction to Theory of Point Processes – Volume 1: Elementrary Theory and Methods,* 2nd edn., Springer.

Guo, Y., Zhuang, J. & Zhou, S., 2015. An improved space-time ETAS model for inverting the rupture geometry from seismicity triggering, *J. geophys. Res.,* **120**, doi:10.1002/2015JB011979.

Helmstetter, A., Kagan, Y.Y. & Jackson, D.D., 2006. Comparison of short-term and time-independent earthquake forecast models for Southern California, *Bull. seism. Soc. Am.,* **961**, 90–106.

Kagan, Y.Y., 1991. Likelihood analysis of earthquake catalogues, *Geophys. J. Int.,* **1061**, 135–148.

Kagan, Y.Y., 2007. Earthquake spatial distribution: the correlation dimension, *Geophys. J. Int.,* **168**(3), 1175–1194.

Mai, P.M., Spudich, P. & Boatwright, J., 2005. Hypocenter locations in finite-source rupture models, *Bull. seism. Soc. Am.,* **95**(3), 965–980.

Marzocchi, W. & Lombardi, A.M., 2009. Real-time forecasting following a damaging earthquake, *Geophys. Res. Lett.,* **36**, L21, 302.

Ogata, Y., 1988. Statistical models for earthquake occurrences and residual analysis for point processes, *J. Am. Stat. Assoc.,* **83**, 9–27.

Ogata, Y., 1998. Space-time point-process models for earthquake occurrences, *Annals of the Institute of Statistical Mathematics,* **50**, 379–402.

Ogata, Y., 2004. Space-time model for regional seismicity and detection of crustal stress changes, *J. geophys. Res.,* **109**(B3), B03308, doi:10.1029/2003JB002621.

Omori, F., 1895. On the aftershocks of earthquakes, *Journal of the College of Science, Imperial University of Tokyo,* **7**, 111–200.

Schoenberg, F.P., 2015. A note on the consistent estimation of spatial-temporal point process parameters, *Statistica Sinica,* in press.

Werner, M.J., Helmstetter, A., Jackson, D.D. & Kagan, Y.Y., 2011. High-resolution long-term and short-term earthquake forecasts for California, *Bull. seism. Soc. Am.,* **101**(4), 1630–1648.

Zhuang, J., 2011. Next-day earthquake forecasts by using the ETAS model, *Earth Planet Space,* **63**, 207–216.

Zhuang, J. & Ogata, Y., 2006. Properties of the probability distribution associated with the largest event in an earthquake cluster and their implications to foreshocks, *Phys. Rev. E,* **73**, 046134, doi:10.1103/PhysRevE.73.046134.

Zhuang, J., Ogata, Y. & Vere-Jones, D., 2002. Stochastic declustering of space-time earthquake occurrences, *J. Am. Stat. Assoc.,* **973**, 369–380.

Zhuang, J., Ogata, Y. & Vere-Jones, D., 2004. Analyzing earthquake clustering features by using stochastic reconstruction, *J. geophys. Res.,* **109**(3), B05301, doi:10.1029/2003JB002879.

Zhuang, J., Chang, C.-P. Ogata Y. & Chen, Y.-I., 2005. A study on the background and clustering seismicity in the Taiwan region by using point process models, *J. geophys. Res.,* **110**(B5), doi:10.1029/2004JB003157.

Zhuang, J., Christophersen, A., Savage, M.K., Vere-Jones, D., Ogata, Y. & Jackson, D.D., 2008. Differences between spontaneous and triggered earthquakes: their influences on foreshock probabilities, *J. geophys. Res.,* **113**(B11), doi:10.1029/2008JB005579.